ISSN 1674-1056
http://cpb.iphy.ac.cn
http://iopscience.iop.org/cpb
中国物理 B
Chinese Physics
中国物理 Chinese Physics B

Influence of intraband motion on the interband excitation andhigh harmonic generation

Rui-Xin Zuo(左瑞欣), Xiao-Hong Song(宋晓红), Xi-Wang Liu(刘希望), Shi-Dong Yang(杨士栋), Wei-Feng Yang(杨玮枫)
Citation: Chin. Phys. B . 2019, 28(9): 094208 . **doi:** 10.1088/1674-1056/28/9/094208
Journal homepage: http://cpb.iphy.ac.cn; http://iopscience.iop.org/cpb

What follows is a list of articles you may be interested in

Resolving multi-orbital effects on high harmonic generation from aligned N_2 molecules in linearly and elliptically polarized intense laser fields

Hong-Jing Liang(梁红静), Xin Fan(范鑫), Shuang Feng(冯爽), Li-Yu Shan(单立宇), Qing-Hua Gao(高庆华), Bo Yan(闫博), Ri Ma(马日), Hai-Feng Xu(徐海峰), Da-Jun Ding(丁大军)
Chin. Phys. B . 2019, 28(9): 094211 . **doi:** 10.1088/1674-1056/28/9/094211

Probing the structure of multi-center molecules with odd-even high harmonics

Ning Su(苏宁), Shujuan Yu(于术娟), Weiyan Li(李卫艳), Shiping Yang(杨世平), Yanjun Chen(陈彦军)
Chin. Phys. B . 2018, 27(5): 054213 . **doi:** 10.1088/1674-1056/27/5/054213

A tunable XUV monochromatic light source based on the time preserving grating selection of high-order harmonic generation

Yong Niu(牛永), Hongjing Liang(梁红静), Yi Liu(刘燚), Fangyuan Liu(刘方圆), Ri Ma(马日), Dajun Ding(丁大军)
Chin. Phys. B . 2017, 26(7): 074222 . **doi:** 10.1088/1674-1056/26/7/074222

All optical method for measuring the carrier envelope phase from half-cycle cutoffs

Li Qian-Guang, Chen Huan, Zhang Xiu, Yi Xu-Nong
Chin. Phys. B . 2014, 23(7): 074206 . **doi:** 10.1088/1674-1056/23/7/074206

Generation of an extreme ultraviolet supercontinuum with a multicycle chirped laser and a static electric field

Zhang Gang-Tai, Bai Ting-Ting, Zhang Mei-Guang
Chin. Phys. B . 2012, 21(11): 114209 . **doi:** 10.1088/1674-1056/21/11/114209

TOPICAL REVIEW — Strong-field atomic and molecular physics

Influence of intraband motion on the interband excitation and high harmonic generation*

Rui-Xin Zuo(左瑞欣)[1,2], Xiao-Hong Song(宋晓红)[1,2,3], Xi-Wang Liu(刘希望)[1,2], Shi-Dong Yang(杨士栋)[1], and Wei-Feng Yang(杨玮枫)[1,2,3,†]

[1] Research Center for Advanced Optics and Photoelectronics, Department of Physics, College of Science, Shantou University, Shantou 515063, China
[2] Department of Mathematics, College of Science, Shantou University, Shantou 515063, China
[3] Key Laboratory of Intelligent Manufacturing Technology (Shantou University), Ministry of Education, Shantou 515063, China

(Received 20 May 2019; revised manuscript received 18 June 2019; published online 23 August 2019)

Tunnelling, acceleration, and collision of electrons are the basic events in the process of high harmonic generation (HHG) in strong-field interaction with atoms. However, the periodic array of atoms in semiconductor structure makes three steps become interatomic coherent process which leads to complicated carrier dynamics and two sources of high harmonic emission: interband polarization and intraband current. The difference of features of high harmonic generation between semiconductors and atoms is strongly linked to the unique presence of intraband motion which manifests itself a nontrivial role in intertwined two dynamics. Here, we review recent experimental and theoretical advances of understanding coupled interband and intraband mechanisms of HHG in semiconductors. Particularly we focus on the influence of intraband motion on the interband excitation, and on the subsequent HHG emission and attosecond pulse generation.

Keywords: high harmonic generation, interband polarization, intraband current, attosecond pulse generation

PACS: 42.65.Ky, 42.65.Re, 72.20.Ht **DOI:** 10.1088/1674-1056/ab3446

1. Introduction

Advances in intense pulse lasers have opened up an avenue to field-induced nonperturbative nonlinear optical phenomena, such as high harmonic generation (HHG) and attosecond pulse generation.[1] Traditionally, the mediators of the strong-field interaction are isolated atoms or small molecules.[2–7] Recently, a range of semiconductors have been used to produce high harmonics when driven by visible,[8] mid-infrared,[9,10] and terahertz[11] fields, allowing for a new spectroscopic technology of reconstructing the electronic band structure[12] and generating pulses with duration of a few tens of attoseconds.[13,14]

Semi-classical three-step model of electrons in atoms offers the fundamental insights into microscopic HHG process.[2] The model comprises tunneling through the bending potential barrier, acceleration of electron in free space and recombination with its associate core. However, the HHG process in semiconductors is much more complicated due to the dense array of atoms in the system.[15–18] The comparison of microscopic mechanisms for atomic and solid-state HHG in both real and momentum space is depicted in Fig. 1.[19] In semiconductor phase, the tunneled electrons undergo scattering by periodic potential, the motion of which is called Bloch oscillation.[20] The electrons would subsequently re-collide with all possible neighboring cations (see Fig. 1(a)). It is transparent to study the solid-state HHG process in momentum space[21,22] since the electronic band structure $\varepsilon(k)$ is formed by the continuum of splitted electronic degenerate states due to the overlapping of electronic wavefunctions in the crystal and the Bloch oscillation is well described as the traversing of electrons across the reciprocal space within bands.[19] For better comparison, the atomic HHG process is also revisited in momentum space (see Fig. 1(d)). The electron is initially in ground state with energy $-I_p$. Upon tunnelling, the electron is freed in the continuum state with zero initial velocity. As the electron is accelerated and decelerated by field force it gains the energy which equals $k(t)^2/2$. The re-collision of electron with the parent ion gives rise to a photon radiation whose energy is $k(t)^2/2+I_p$.[2] In solid state, take a two-band model as example, the tunneling step can be viewed as the creation of electron–hole pairs which mainly occurs around $k=0$ and vertical interband transition for electrons overcoming the energy gap. Subsequently, the electron and hole move in respective conduction and valence bands with the same instantaneous momentum value. The velocity and energy of intraband motion is constrained by the band structure of semiconductors. The photon is radiated upon the electron transiting back to the valence band and recombining with its associate hole with energy equal to the band gap $\varepsilon(k)$ of instantaneous k (see Fig. 1(b)). Therefore, there are two possible sources

*Project supported by the National Natural Science Foundation of China (Grant Nos. 11674209 and 11774215), the High Level University Projects of Guangdong Province of China (Mathematics, Shantou University), and the Open Fund of the State Key Laboratory of High Field Laser Physics (SIOM), China. WFY and XHS acknowledge support of the Department of Education of Guangdong Province, China (Grant No. 2018KCXTD011).

†Corresponding author. E-mail: wfyang@stu.edu.cn

© 2019 Chinese Physical Society and IOP Publishing Ltd

of HHG: the radiation from intraband current and interband polarization.[23,24,26] There is no analogous intraband emission in atomic phase.

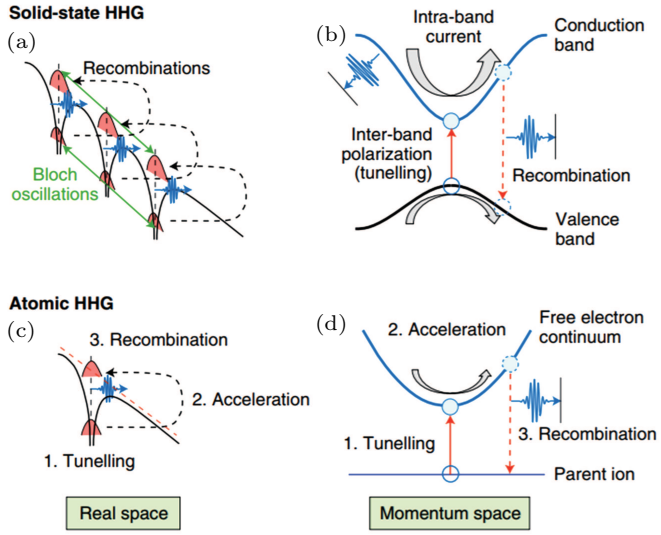


Fig. 1. (a)–(c) The real-space picture of solid-state and atomic HHG. In (c) three-step recollision model of atomic HHG includes tunelling, acceleration and recombination whereas in (a) tunnelled electrons scattered by periodic Coulomb potential and they could collide with not only its parent ion but also neighboring ions. (b)–(d) The picture of solid-state and atomic HHG in momentum space. In panel (d) tunneled electron accelerates freely in continuum state and recombines with its parent ion whereas in panel (b) two-band model of solid-state HHG where both interband polarization and intraband current could emit high-harmonic radiation. Adapted from Ref. [19].

The first experiment of HHG was observed in bulk ZnO crystal[9] exposed to mid-infrared laser pulse, marking the breakthrough of research in HHG from semiconductors. The observed harmonics spectrum extends well beyond the band edge of the crystal which manifests the significant effect of Bloch oscillation to the nonlinearities of radiation and validates the linear scaling of the harmonic cut-off energy to the field amplitude. Besides, the experiment of terahertz-induced HHG from GaSe[11,25] demonstrates that dynamical Bloch oscillation contributes considerably to the HHG process and leads to the appearance of second plateau in the HHG emission spectrum. Bloch frequency, $\omega_{\rm B} = eE_0a/\hbar$ for Bragg scattering defines the rate at which a classical electron travels through the Brillouin zone (BZ) for static field with the strength E_0 and lattice constant a if scattering is neglected. It is revealed that the emitted extreme ultraviolet (EUV) radiation in SiO_2 comes from multi-petahertz frequency of intraband current.[8] These studies indicate the association of high harmonics emission with intraband current. However, interband contributions could also lead to a linear scaling of harmonic cutoff energy with the field amplitude and exhibits a dominance over other competing mechanisms for above band gap harmonics.[26–28] The behavior of HHG spectrum in semiconductors cannot be fully explained by separated mechanism of interband or intraband dynamics. Based on the re-collision picture proposed by Vampa *et al.*,[27] an interferometry approach has been brought up by applying two-color field to reconstruct the target band structure. In this scheme, both the two mechanisms are involved where the band information is encoded in the trajectory of electron–hole pair in the momentum space but the termination of the intraband motion is manifested by the phase of interband even harmonics radiation. Momentum-resolved band structure can be obtained by analysing difference of unbalanced intraband motion in reversed crystal direction.[10] The influence of coherent interband and intraband mechanisms vary from a series of targets and conditions of subjected laser fields, the microscopic process of solid-state HHG has not been fully understood.

In this Review, we begin with the theoretical methods of describing and analysing HHG from semiconductors. Then we present an overview of recent progress of understanding intraband motion effect on the behavior of interband excitation in the coherent microscopic process and outcome of harmonic emission. Lastly we summarize works with regard to difference of HHG process between semiconductors and atoms.

2. Theoretical method

For the optically excited materials description, the relevant physical quantities are the microscopic polarization $p_k^{\lambda\lambda'} = \langle \hat{a}^\dagger_{\lambda,k}\hat{a}_{\lambda,k}\rangle$, where $\hat{a}^\dagger_{\lambda,k}$ ($\hat{a}_{\lambda,k}$) is annihilation (creation) operator for an electron with momentum k in band λ, i.e., the corherent transition amplitude between two different bands $\lambda \neq \lambda'$, and the carrier occupation f_k^λ in band λ. The derivation of the dynamical evolution of these quantities described by SBEs starts from the Heisenberg equation

$$\mathrm{i}\hbar\frac{\partial \hat{a}_{\lambda,k}(t)}{\partial t} = [\hat{a}_{\lambda,k}(t), \hat{H}]. \tag{1}$$

A more detailed discussion is provided in Ref. [29].

The two-band SBEs read

$$\mathrm{i}\hbar\frac{\partial}{\partial t}p_k^{cv} = \left(\varepsilon_k^c - \varepsilon_k^v - \mathrm{i}\frac{\hbar}{T_2}\right)p_k^{cv} - \Omega_{\rm R}(k)(f_k^v - f_k^c) + \mathrm{i}\,|e|E(t)\nabla_k p_k^{cv}, \tag{2}$$

$$\hbar\frac{\partial}{\partial t}f_k^{c(v)} = -2\,\mathrm{Im}\left[\Omega_{\rm R}(k)(p_k^{cv})^*\right] + |e|E(t)\nabla_k f_k^{c(v)}, \tag{3}$$

where T_2 is the dephasing time. The Rabi frequency $\Omega_{\rm R}(k) = d_{cv}(k)E(t)/\hbar$,[30] with the dipole moment $d_{cv}(k)$. The terms with ∇_k describe the instantaneous acceleration of carriers and polarization by $E(t)$. An advantage of SBEs is that the terms containing ∇_k can be selectively included or removed in the numerical computation to analyze the dynamics of intraband motion. The full form of SBEs for any multi-band system can be found in Ref. [11]. In addition to the polarization source,

$$P(t) = \sum_{k,\lambda,\lambda'}\left[d_k^{\lambda\lambda'}p_k^{\lambda\lambda'} + \text{c.c.}\right], \tag{4}$$

which is identical in atomic systems, the radiation emitted from current source created by the acceleration of carriers is defined by

$$J(t) = \sum_{k,\lambda} |e| v_k^\lambda n_k^\lambda, \tag{5}$$

where v_k^λ is the band velocity and $v_k^\lambda = \frac{|e|}{\hbar}\nabla_k \varepsilon_k^\lambda$. The total high harmonic spectrum in frequency domain is obtained from the Fourier transform of $\frac{\partial}{\partial t}P(t)+J(t)$

$$I_{\rm rad}(\omega) = |\omega P(\omega) + {\rm i}J(\omega)|^2. \tag{6}$$

Analyzing a temporal or spatial signal in frequency domain to gain more properties is applied extensively in the field of image processing. Here we review the development of time–frequency methods. Fourier transform (FT) is the basic algorithm and its integration goes over the whole time domain and the resulting signal contains the statistic property of frequency, one cannot know the exact moment of generating a signal with any frequency. To overcome the drawback of FT, new algorithms based on the idea of short time FT have been proposed since 1940s, like Gabor transform (GT)[31] and wavelet transform (WT).[32] For a temporal signal $f(t)$, GT is defined by

$$G_f(a,b,\omega) = \int_{-\infty}^{\infty} f(t) g_a(t-b) {\rm e}^{-{\rm i}\omega t} {\rm d}t, \tag{7}$$

where $g_a(t-b)$ is a temporal localized window function which is usually chosen to be Gaussian function whose width is a and the window function slides along time axis with parameter b which would cover the entire time domain. GT gives the localized information of signal in time and frequency domain simultaneously. WT is defined by

$$W_f(a,b) = \frac{1}{\sqrt{|a|}} \int_{-\infty}^{\infty} f(t) \Psi\left(\frac{t-b}{a}\right) {\rm d}t, \tag{8}$$

where $\Psi(\frac{t-b}{a})$ is the wavelet function with a flexible window varying its width with the frequency. WT possesses higher resolution of frequency than GT.

However, the uncertainty relation of time and frequency characteristics is inherent to these transforms. The synchrosqueezing transform (SST)[33] is proposed to lower the uncertainty greatly. SST is a kind of post-processing method by reassigning the coefficients in frequency[34] and is originally introduced in the context of continuous wavelet transform (CWT),[35] which is defined by

$$S_f(\omega,b) = \int V_f(a,b) \delta(\omega - \hat{\omega}_f(a,b)) {\rm d}a, \tag{9}$$

where $V_f(a,b)$ is the CWT result of a temporal signal. $\hat{\omega}_f(a,b)$ is the local instantaneous frequency defined by

$$\hat{\omega}_f(a,b) = \frac{\partial_b V_f(a,b)}{2\pi {\rm i} V_f(a,b)}. \tag{10}$$

CWT-based SST is firstly applied in strong-field physics to analyze near- and below-threshold high-order harmonics of atoms which validates the possible semiclassical analysis and is better to understand working mechanisms for below-threshold generations.[36] Although SST is a powerful tool in analyzing instantaneous properties, due to the wave shape functions used in CWT is band-limited and the low resolution in high frequency part, CWT-based SST would not be suitable to address the problem in the circumstances requiring high resolution in low and high frequency part of time–frequency analysis at the same time. Synchrosqueezing with the short-time Fourier transform (SSTFT)[37] has been proposed to address this problem but it is not suitable to estimate instantaneous high frequency accurately. All problems above are overcame by synchrosqueezed wave packet transform (SSWPT)[37,38] which is capable of estimating a wide band of instantaneous frequency accurately and has a better resolution to distinguish high frequency harmonic than the CWT-based SST. A geometric parameter s is used to define a family of wave packets $\omega_{ab} : |a| \geq 1, b \in R$ with $s \in (1/2, 1)$

$$\omega_{ab}(t) = |a|^{s/2} \omega(|a|^s (t-b)) {\rm e}^{2\pi {\rm i}(t-b)a}. \tag{11}$$

The WPT of a function $f(t)$ is given by

$$W_s(a,b) = \langle \omega_{ab}, f \rangle = \int \overline{\omega_{ab}(t)} f(t) {\rm d}t. \tag{12}$$

The instantaneous frequency information function of $f(t)$ is defined by

$$\omega_s(a,b) = \frac{\partial_b W_s(a,b)}{2\pi {\rm i} W_s(a,b)}. \tag{13}$$

Given $f(t)$, $W_s(a,b)$, and $\omega_s(a,b)$, the time–frequency distribution of SSWPT is defined by

$$T_s(\omega,b) = \int_{a:W_s(a,b)\neq 0} |W_s(a,b)|^2 \delta({\rm Re}\omega_s(a,b) - \omega) {\rm d}a. \tag{14}$$

Given that more adjustable parameters in SSWPT one is encouraged to apply it in strong field physics, particularly HHG, to get a detailed and accurate information of radiation distribution in time–frequency plane.

3. The influence of intraband motion on the interband excitation in resonant interaction

In the previous investigations of resonant nonperturbative extreme nonlinear optics, it is usually thought that the interband transition near the band gap in semiconductors to a great extent decides the nonlinear optical response, such as carrier-wave Rabi flopping (CWRF), and the intraband dynamics can be neglected in theoretical analysis.[39,40] However, the recent studies have shown that the intraband current is strong and leads to a occupation distribution of conduction band in a large

fraction of Brillouin zone even in the CWRF regime where $\Omega_R \approx \omega_0$.[41]

Since the interband transition rate decreases exponentially with increasing energy gap, the analysis of population dynamics initially excited from Γ point can intuitively approximate the essence of microscopic quantum process of HHG. In Ref. [41], it is found that for a ZnO crystal resonantly driven by an infrared laser pulse, the time evolution of electron population in the lowest conduction band (c_1) exhibits a novel kicked anharmonic Rabi oscillation. As illustrated in Fig. 2(a),[41] the c_1 is populated and depopulated rapidly in an ultrashort time window centered at the crest of electric field, which is indicated by dots on the curves, and it keeps flat between these moments. For the selected trajectory in momentum space starting from the Γ point, the symmetric intraband motion makes the profile of Rabi oscillation evident (see blue solid curve). In resonant excitation case, the Rabi oscillation makes the deexcitation in the later half Rabi cycle balance with excitation in the former one and result in the lower value of occupation in the conduction at the end of laser pulse. The effect of kicked anharmonic Rabi oscillation can be easily understood since at the peak of electric field, electrons are injected into c_1 mostly around the Γ point. As time goes by, though electrons in c_1 is driven away to further region of Brillouin zone, the weakened field strength and wider bandgap determine that it is hard for interband excitation with instantaneous $k(t)$, thus no more increase for $n_{c_1}[K(t),t]$, but it surges again once the electron is driven back to the Γ point by the electric field.[41]

In Ref. [42], it was further demonstrated that the intraband motion can dramatically affect the interband excitation. As stated in the abstract of the paper, "Surprisingly, we found that despite the resonant driving laser, the optical response during the light–matter interaction is dominated by intraband motion." It is manifested that the HHG in ZnO crystal induced by pump pulse with similar parameters of that in Ref. [41], the analogous behavior for carrier dynamics of k-integrated conduction band occupation (as displayed in Fig. 2(b)) that a rapid interband transition occurs only at the crest of driven field due to the coupled interband and intraband mechanisms is obvious. This leads to a significant enhancement of photo-excited carriers at the end of the pulse compared to the interband limit. The intraband motion can not only accelerate carriers within the same band, its coupling with the interband mechanism greatly influence the behavior of interband transition.

All these studies demonstrate that the intraband motion plays an non-negligible role in carriers transition among bands which is quiet different from atomic case. According to the semi-classical analysis in atoms, the ionization takes place at $k = 0$ and the transition rate is only sensitive to the external field, the weight of a classical trajectory is fixed during the free acceleration in the continuum state.[43–46] In the HHG process of semiconductors, the instantaneous population of electron–hole pair is sensitive to the field strength and energy band during the intraband motion.

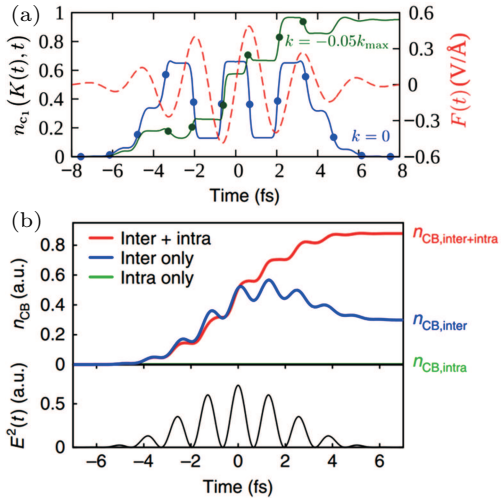


Fig. 2. (a) Time-resolved electronic population in the lowest conduction for selected reciprocal-space pathways. The starting point is $k = 0$ for the blue curve and $k = -0.05k_{max}$ for the green curve. The dots on both curves denote the moments when the electrons pass through the Γ point. The dashed red curve shows the electric field whose central frequency is resonant with the bandgap of GaAs. Adapted from Ref. [41]. (b) Calculated k-integrated population dynamics for coupled interband and intraband mechanism case (red curve), pure interband case (blue cure), and pure intraband case (green curve). The parameters of electric field are much close to that in (a). Adapted from Ref. [42].

4. CEP dependence of HHG emission

Recently, a strong CEP dependence of far-from-resonantly excited HHG from wide-gap MgO crystal has been observed experimentally[47] (see Fig. 3(a)). It originates from the sub-cycle chirp of the emission dynamics due to the short duration of the pulse since the amplitude and phase of bursts are sensitive to the instantaneous value of the laser potential.[48–50] The HHG emission is attributed to interband mechanism since it has been demonstrated that only interband emission shows the frequency atto-chirp effect whereas intraband process shows no frequency chirp effect.[48]

However, recent investigation[51] shows that even in this case, the intraband motion plays a crucial role on the CEP dependence of HHG in MgO crystal. It is illustrated that in the calculation of HHG with field amplitude $E_0 = 1.3$ V/Å and wavelength $\lambda = 1.7$ μm, the CEP shift of the photon energy above band gap can be clearly seen (see Fig. 3(b)) which is identical with that of Fig. 2(b) in Ref. [47]. Surprisingly, the CEP-dependent energy shift disappears when intraband motion is artificially switched off (see Fig. 3(c)). It is shown that in contrast to that the total emission in the plateau region is dominated by interband polarization when considering coupling effect, the harmonic spectrum is at least 5 orders of magnitude lowered and only 1st and 3rd harmonics are left in the absence of intraband motion (see Fig. 4(a)). The time-dependent population increases smoothly in every half

cycle for pure interband case (see Fig. 4(b)). However, the dynamical population of selected path starting from Γ point in conduction band $n_C[K(t),t]$ increases rapidly at the crests of electric field when $A(t) \approx 0$ and followed by keeping constant for about half-cycle time in the presence of intraband motion, which means that the kicked transition observed in resonant interaction can also occur for non-resonant case. This nontrivial carrier dynamics is called carrier-wave population transfer (CWPT). Different from the case in resonant regime, the time-dependent population shows no signature of Rabi flopping in MgO crystal, which is not expected to happen in non-resonant excitation case.

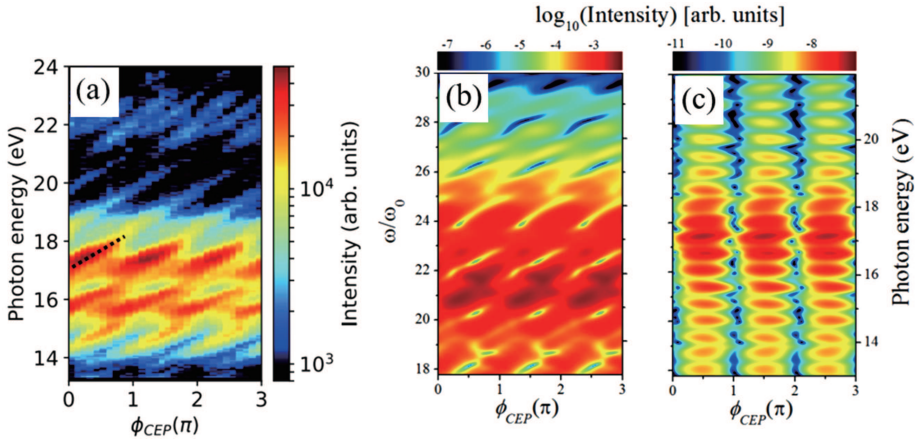


Fig. 3. (a) Experimentally measured CEP dependence of HHG emission from MgO crystal. Adapted from Ref. [47]. (b) Simulated results of panel (a). (c) Same computation of (b) but in the absence of intraband motion. Adapted from Ref. [51].

It is demonstrated that the temporal confinement of interband excitation by intraband motion still exists for longer duration (see Figs. 4(c)–4(e)).[51] It is evident that in contrast to the harmonics below band gap, every individual harmonic in HHG plateau region is broadened for $\tau_p = 10T_0$ (see Fig. 4(c)), which is the inevitable result of the confinement of interband transition of carriers on the attosecond time scale. Shorter pulse, for example $\tau_p = 4T_0$, further broadens the harmonics and adjacent odd harmonics meet and interfere with each other. Small peaks around the position of even harmonics are consequently generated (see Fig. 4(e)). Particularly for $\tau_p = 2T_0$ case, the doubled broadening effect is strong enough to make every tail of odd harmonics overlap even with adjacent odd ones and the range of interference gets large. The amplitude of generated small peaks is comparable with odd harmonics whose energy is sensitive to the change of CEP resulting from different phases of neighboring harmonics. Hence, the HHG spectrum is complicated (see Fig. 4(a)) and the energy shift versus CEP spans across all odd and even harmonics in the plateau region (see Figs. 3(a) and 3(b)).

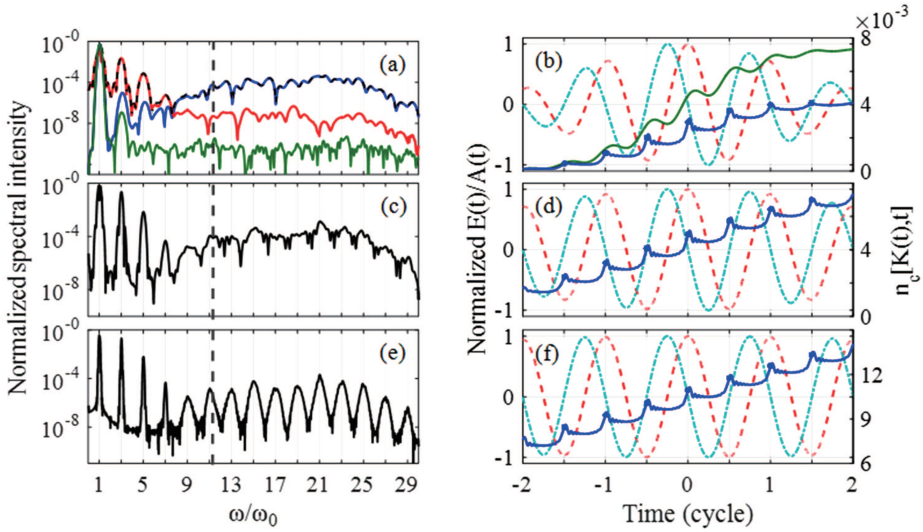


Fig. 4. (a) The total HHG spectrum I_{rad} (black dash line), interband polarization I_{rad}^{pol} (blue solid line), and intraband current I_{rad}^{curr} (red solid line) for coupled inter- and intraband dynamics, and pure interband HHG (green solid line) when the intraband motion is artificially switched off with field strength 1.3 V/Å and CEP = 0. (b) The corresponding time-dependent population $n_C[K(t),t]$ for coupled (blue line) and pure interband (green line) motion. The red dash and glaucous dot-dash lines in panel (b) shows the normalized electric field and vector potential, respectively. The blue dots on the curves in panel (b) denote moments when the electrons pass through the Γ point. Panels (c) and (d) are the same as panels (a) and (b) but for $\tau_p = 10T_0$. Panels (e) and (f) are the same as panels (a) and (b) but for $\tau_p = 4T_0$. Adapted from Ref. [51].

It is counterintuitive to find that in contrast to the case of pure interband mechanism, the population of conduction band for coupled process is lowered at the end of pulse due to the CWPT effect, but leads to the higher efficiency of harmonic emission. The temporal confinement of interband excitation within each half cycle facilitates the constructive interference among the quantum carriers in the transition process and consequently enhance the nonlinear interband polarization and makes it the dominant contribution to the total HHG.[51] The influence of intraband motion on the interband excitation is universal and intensively influence the behavior of high harmonics emission.

5. Difference between atomic and solid-state HHG

It is revealed that the temporal confinement of interband excitation happens roughly upon the moments when the vector potential equals to zero at the crest of electric field.[51] For HHG induced by a tailored two-color pulse like $E(t) = [E_0 \cos(\omega_0 t) + 0.25E_0 \cos(\frac{1}{3}\omega_0 + \phi)]f(t)$ with fundamental field is the same as that in Fig. 2, the only one robust interband promotion for $\phi = 0$ is observed synchronizing with the peak of applied field whereas the excitation is heavily suppressed in other half cycles.[51] The spectrally integrated of plateau region (black line in Fig. 5(c)) as well as spectrally resolved (color map in the time–frequency distribution in Fig. 5(e)) burst is emitted at the moment delayed for about 1/4 optical cycle with respect to the field peak. The excitation and the burst emission in the central half cycle suggests the unique correlation of these two events (indicated by black line with arrow). It is confirmed by the observed two pairs of excitation and harmonic pulse bursts for the case $\phi = \pi$ and the relative strength of emitted photon energy is roughly scaled with the amplitude of the associated excitation. It is concluded that the photons are emitted upon re-collision of electron–hole pairs which excurse for about 1/4 optical cycle after their creation (see Figs. 5(d) and 5(f)). This is quite different from the HHG process in atomic system predicted by three-step model where about 3/4 optical cycle is needed that the electron is pulled back and recombines with the core.[1]

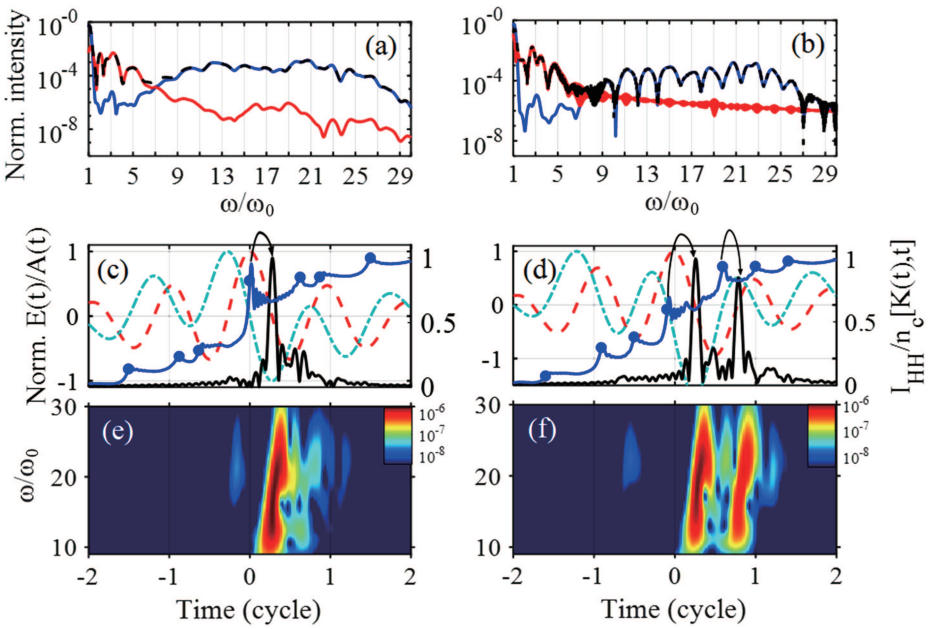


Fig. 5. (a) HHG spectrum for the two-color field with relative phase $\phi = 0$. The corresponding time-dependent population (blue curve with dots) and attosecond pulse field emission spectrally integrated of 10–30th are shown in panel (c) and time–frequency analysis of emission is depicted in panel (d). (b), (d), and (f) are the same as panels (a), (c), and (e), but for $\phi = \pi$. Adapted from Ref. [51].

The deviation of time profile of solid-state HHG process from atomic case embodies the spatial delocalization of Bloch electrons in the strong-field limit.[52,53] In Ref. [52], the HHG yield exhibits anisotropic angular distribution for a linear polarized pump in MgO crystal. The underlying origin is assumed to be coherent collisions of Bloch electrons with neighboring atomic sites in periodic solids and is qualitatively validated based on the simple semi-classical electron trajectory analysis. This is further justified by the strong laser ellipticity dependence of HHG. It is found that the highest and secondary highest HHG efficiency occur when the trajectories are driven to traverse across the Mg–O and Mg–Mg (or O–O) sites with large electronegativity gradient for charge transfer along these bonding directions. The minimum happens when the electron trajectories are collision-free. The period for trajectories connecting Mg–O sites along the X–Γ–X crystal direction would be much shorter than 3/4 optical cycle needed in atomic case and 1/4 optical cycle is assumed to be the coherent result of trajectories from all unit cells. By connecting time-resolved excitation together with emission dynamics and coherent col-

lisions of the delocalized electrons with the interatomic potential in real space, we identify the inherent consistency of temporal and spatial characteristics in the microscopic process of solid-state HHG.

6. Conclusion and outlook

We review the recent investigations of coupled interband polarization and intraband motion dynamics in solid-state HHG. The reported critical temporal confinement of interband excitation effect is common in semiconductors regardless of excitation parameters. The effect intuitively interprets the domination of interband polarization in the emission owing to the intraband motion and can greatly enhance extreme nonlinear optical effects. The interband excitation is sensitive to both electric field and vector potential condition and the emission is 1/4 optical cycle delayed which is related to the delocalization process in real space. The unusual temporal structure of interband excitation and harmonic pulse generation in solid allows controlling of ultrafast carrier dynamics on the level of carrier wave by tuning the waveform of multi-color field. For the tailored two-color field with $\phi = 0$ in Ref. [51] the spectra is notablely modulated and the smooth ultrabroad supercontinuum covering the almost the entire plateau region is obtained, which provides perfect source of isolated attosecond pulse. We expect to take full advantage of time–frequency analysis tool with high resolution in the low frequency region to uncover the physical origin of harmonic emission whose energy below the minimum band gap.

References

[1] Krausz F and Ivanov M 2009 *Rev. Mod. Phys.* **81** 163
[2] Corkum P B 1993 *Phys. Rev. Lett.* **71** 1994
[3] L'Huillier A and Balcou P 1993 *Phys. Rev. Lett.* **70** 774
[4] Wang L, Wang G, Jiao Z, Zhao S and Zhou X 2018 *Chin. Phys. B* **27** 073205
[5] Yang W, Song X, Zeng Z, Li R and Xu Z 2010 *Opt. Express* **18** 2558
[6] Su N, Yu S, Li W, Yang S and Chen Y 2018 *Chin. Phys. B* **27** 054213
[7] Zhang H D, Guo J, Shi Y, Du H, Liu H F, Huang X R, Liu X S and Jing J 2017 *Chin. Phys. Lett.* **34** 014206
[8] Luu T T, Garg M, Krruchinin S Yu, Moulet A, Hassan M Th and Goulielmakis E 2015 *Nature* **521** 498
[9] Ghimire S, DiChiara A D, Sistrunk E, Agostini P, DiMauro L F and Reis D A 2011 *Nature* **7** 138
[10] Vampa G, Hammond T J, Thiré N, Schmidt B E, Légaré F, McDonald C R, Brabec T and Corkum P B 2015 *Nature* **522** 462
[11] Schubert O, Hohenleutner M, Langer F, Urbanek B, Lange C, Huttner U, Golde D, Meier T, Kira M, Koch S W and Huber R 2014 *Nat. Photon.* **8** 119
[12] Vampa G, Hammond T J, Thiré N, Schmidt B E, Légaré F, McDonald C R, Brabec T, Klug D D and Corkum P B 2015 *Phys. Rev. Lett.* **115** 193603
[13] Hammond H J, Monchoché S, Zhang C, Vampa G, Klug D, Naumov A Yu, Villevenue D M and Corkum P B 2017 *Nature Photon.* **11** 594
[14] Krausz F and Stockman M I 2014 *Nature Photon.* **8** 205
[15] Zhao K, Xu S Y, Jiang Y J, Gao Y T, Liu Y Y, He P, Teng H, Zhu J F and Wei Z Y 2018 *Acta Phys. Sin.* **67** 214205 (in Chinese)
[16] Cai H P, Gao J, Li B Y, Liu F, Chen L M, Yuan X H, Chen M, Sheng Z M and Zhang J 2018 *Acta Phys. Sin.* **67** 124203 (in Chinese)
[17] Song X, Hao Z, Yan M, Wu M and Yang W 2015 *Laser Phys. Lett.* **12** 105003
[18] Song X, Yan M, Wu M, Sheng Z, Hao Z, Huang C and Yang W 2015 *Journal of Optics* **17** 055503
[19] Ghimire S and Reis D A 2019 *Nature* **15** 10
[20] Bloch F Z 1929 *Physik* **52** 555
[21] Kittel C 1963 *Quantum Theory of Solids* (New York: Wiley)
[22] Meier T, Thomas P and Koch S W 2007 *Coherent Semiconductor Optics* (Berlin: Springer)
[23] Meier T, von Plessen G, Thomas P and Koch S W 1994 *Phys. Rev. Lett.* **73** 902
[24] Meier T, Rossi F, Thomas P and Koch S W 1995 *Phys. Rev. Lett.* **75** 2558
[25] Hohenleutner M, Langer F, Schubert O, Knorr M, Huttner U, Koch S W, Kira M and Huber R 2015 *Nature* **523** 572
[26] Golde D, Meier T and Koch S W 2008 *Phys. Rev. B* **77** 075330
[27] Vampa G, McDonald C R, Orlando G, Klug D D, Corkum P B and Brabec T 2014 *Phys. Rev. Lett.* **113** 073901
[28] Higuchi T, Stockman M I and Hommelhoff P 2014 *Phys. Rev. Lett.* **113** 213901
[29] Haug H and Koch S W 2004 *Quantum Theory of the Optical and Electronic Properties of Semiconductors* (World Scientific)
[30] Cundiff S T, Knorr A, Feldmann J, Koch S W, Göbel E O and Nickel H 1994 *Phys. Rev. Lett.* **73** 1178
[31] Gabor D 1946 *J. Ins. Electr. Eng.* **93** 429
[32] Grossmann A and Morlet J 1984 *SIAM J. Math. Anal.* **15** 723
[33] Daubechies I and Maes S 1996 *Wavelets in Medicine and Biology* (New York: Taylor & Francis Group)
[34] Auger F and Flandrin P 1995 *IEEE Transactions on Signal Processing* **43** 1068
[35] Daubechies I, Lu J and Wu H T 2011 *Appl. Comput. Harmon. Anal.* **30** 243
[36] Li P C, Sheu Y L, Laughlin C and Chu S I 2014 *Phys. Rev. A* **90** 041401(R)
[37] Yang H 2015 *Appl. Comput. Harmon. Anal.* **39** 33
[38] Thakur G and Wu H T 2011 *SIAM J. Math. Anal.* **43** 2078
[39] Mücke O D, Tritschler T, Wegener M, Morgner U and Kärtner F X 2002 *Phys. Rev. Lett.* **89** 127401
[40] Tritschler T, Mücke O D and Wegener M 2003 *Phys. Rev. A* **68** 033404
[41] Wismer M S, Kruchinin S Y, Ciappina M, Stockman M I and Yakovlev V S 2016 *Phys. Rev. Lett.* **116** 197401
[42] Schlaepfer F, Lucchini M, Sato S A, Volkov M, Kasmi L, Hartmann N, Rubio A, Gallmann L and Keller U 2018 *Nat. Phys.* **14** 560
[43] Song X, Shi G, Zhang G, Xu J, Lin C, Chen J and Yang W 2018 *Phys. Rev. Lett.* **121** 103201
[44] Gong X, Lin C, He F, Song Q, Lin K, Ji Q, Zhang W, Ma J, Lu P, Liu Y, Zeng H, Yang W and Wu J 2017 *Phys. Rev. Lett.* **118** 143203
[45] Song X, Lin C, Sheng Z, Liu P, Chen Z, Yang W, Hu S, Lin C D and Chen J 2016 *Sci. Rep.* **6** 28392
[46] Lin C, Zhang H T, Sheng Z, Yu X, Liu P, Xu J, Song X, Hu S, Chen Z and Yang W 2016 *Acta Phys. Sin.* **65** 223200 (in Chinese)
[47] You Y S, Wu M, Yin Y, Chew A, Ren X, Gholam-Mirzaei S, Browne D A, Chini M, Chang Z, Schafer K J, Gaarde M B and Ghimire S 2017 *Opt. Lett.* **42** 1816
[48] Wu M, Ghimire S, Reis D A, Schafer K J and Gaarde M B 2015 *Phys. Rev. A* **91** 043839
[49] Wu M, Browne D A, Schafer K J and Gaarde M B 2016 *Phys. Rev. A* **94** 063403
[50] Yang W, Song X, Gong S, Cheng Y and Xu Z 2007 *Phys. Rev. Lett.* **99** 133602
[51] Song X, Zuo R, Yang S, Li P, Meier T and Yang W 2019 *Opt. Express* **116** 2225
[52] You Y S, Reis D A and Ghimire S 2017 *Nat. Photon.* **13** 3995
[53] Liu L, Zhao J, Dong W, Liu J, Huang Y and Zhao Z 2017 *Phys. Rev. A* **96** 053403